

Probing Light Thermal Dark-Matter With a Higgs Portal Mediator

Gordan Krnjaic^{1,*}

¹*Fermi National Accelerator Laboratory, Batavia, IL, 60510, United States*
(Dated: November 2, 2016)

We systematically study light ($< \text{few GeV}$) Dark Matter (DM) models that thermalize with visible matter through the Higgs portal and identify the remaining gaps in the viable parameter space. Such models require a comparably light scalar mediator that mixes with the Higgs to avoid DM overproduction and can be classified according to whether this mediator decays (in)visibly. In a representative benchmark model with Dirac fermion DM, we find that, even with conservative assumptions about the DM-mediator coupling and mass ratio, the regime in which the mediator is heavier than the DM is fully ruled out by a combination of collider, rare meson decay, and direct detection limits; future and planned experiments including NA62 can further improve sensitivity to scenarios in which the Higgs portal interaction does not determine the DM abundance. The opposite regime in which the mediator is lighter than the DM and the latter annihilates to pairs of visibly-decaying mediators is still viable, but much of the parameter space is covered by rare meson decay, supernova cooling, beam dump, and direct detection constraints. Nearly all of these conclusions apply broadly to the simplest variations (e.g. scalar or asymmetric DM). Future experiments including SHiP, NEWS, and Super-CDMS SNOLAB can greatly improve coverage to this class of models.

I. INTRODUCTION

Although evidence for the existence of Dark Matter (DM) is overwhelming, its particle identity remains unknown and discovering its short distance properties is a top priority in fundamental physics. This task is especially daunting because viable DM candidate masses span dozens of orders of magnitude with different cosmological histories and phenomenological consequences. However, if dark and visible matter achieve thermal equilibrium in the early universe, the viable mass range is much narrower, $m_{\text{DM}} \sim \text{keV} - 100 \text{ TeV}$; below a few keV, DM is too hot for structure formation and above $\sim 100 \text{ TeV}$, DM is in tension with perturbative unitarity. Thermal contact also generically overproduces DM in the early universe, so such scenarios require a depletion mechanism to yield the observed abundance. This feature motivates appreciable non-gravitational interactions with visible matter and serves as a well motivated and largely model-independent organizing principle for the broad DM discovery effort.

For the upper half of the thermal window, $m_{\text{DM}} \sim \text{GeV} - 100 \text{ TeV}$, DM can carry electroweak quantum numbers and annihilate via Standard Model (SM) interactions. For the lower half, $m_{\text{DM}} \sim \text{keV} - \text{GeV}$, thermal dark matter with weak-scale (or weaker) interactions is overproduced in the early universe [1], so viable scenarios require additional, SM neutral mediators to deplete the overabundance. Unless SM fields are charged directly under additional forces (e.g. $U(1)_{B-L}$), these mediators will mix with the SM through at least one of the renormalizable “portal” operators

$$HL, B^{\mu\nu}, H^\dagger H, \quad (1)$$

where L is a lepton doublet, $B^{\mu\nu}$ is the hypercharge field strength tensor, and H is the Higgs doublet.

Stable thermal DM interacting through the lepton portal, HL , is difficult to engineer because either the DM decays through this interaction (e.g. DM is a right handed or sterile neutrino) or the mediator is fermionic and SM-DM scattering is proportional to neutrino masses so the two sectors never thermalize (see [2] for a review). Vector mediators can kinetically mix with $B^{\mu\nu}$ and there is a growing effort to test this scenario [3–16].

In this paper we study a simple class of light ($< \text{few-GeV}$) thermal DM models with a singlet scalar mediator that mixes with the SM through the Higgs portal. For a singlet mediator Φ , the mixing arises from the renormalizable operators

$$\mathcal{L}_{\Phi,H} = (A_{\Phi H} \Phi + \lambda_{\Phi H} \Phi^2) H^\dagger H. \quad (2)$$

After electroweak symmetry breaking, diagonalizing the scalar mass terms that arise from Eq. (2) yields mass eigenstates ϕ and h , which we identify as the DM-SM mediator and the Higgs boson, respectively (see Appendix A for a discussion). Our representative benchmark scenario consists of a Dirac fermion DM candidate coupled to the mediator ϕ via

$$\mathcal{L}_{\phi,\text{DM}} = \phi(g_\chi \bar{\chi}\chi + g'_\chi \bar{\chi}\gamma^5\chi), \quad (3)$$

where g_χ and g'_χ are the parity even and odd couplings, respectively. However, as we will see below, the relevant physics for light DM is captured by the scalar interaction, so we will omit parity odd coupling g'_χ from our benchmark without loss of essential generality (see discussion in Sec. VII).

Since Φ mixes with the scalar component of H (the Higgs boson, h), it acquires a coupling to SM fermions, which we parametrize with the mixing angle $\sin\theta$ and expand in the mass basis to obtain the mediator interaction

$$\mathcal{L}_{\phi,\text{SM}} = \phi \sin\theta \sum_f \frac{m_f}{v} \bar{f} f, \quad g_f \equiv \frac{m_f}{v} \sin\theta, \quad (4)$$

where f is a SM fermion of mass m_f and $v \simeq 246 \text{ GeV}$ is the SM Higgs vacuum expectation value. Although this is only

* krnjaicg@fnal.gov

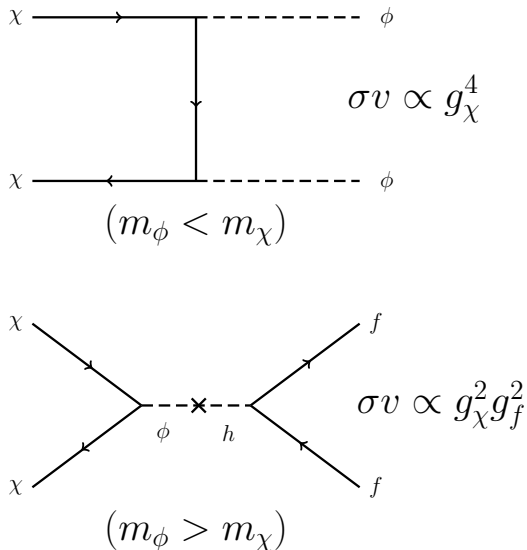


FIG. 1. Leading Feynman diagrams giving rise to χ annihilation in the early universe. If $m_\chi > m_\phi$ the annihilation is predominantly through the t -channel and the mediator decays into SM states via Higgs mixing. If $m_\chi < m_\phi$, DM annihilates directly to SM fermions through the s channel which depends on the SM-mediator coupling and is the most predictive scenario; If $m_\phi > 2m_\chi$ the ϕ will decay invisibly to dark matter. In the $2m_\chi > m_\phi > m_\chi$ regime, it may also be possible to annihilate through the forbidden channel [17]

one of many scenarios for DM interacting through the Higgs portal, it captures much of the essential physics, so most of the constraints and projections will apply to a much broader class of variations on this simple setup.

Light DM interacting through the Higgs portal has been considered before in the context of minimal DM coupled directly to the portal [18], as a byproduct of Higgs decays [19], as pair produced in rare B and K decays [20], as coupled to a scalar mediator mixed with the Higgs [21–23], as a sub-eV non thermal candidate [24]. The bounds on a light, Higgs portal scalar in the context of self-interacting DM were considered in [25, 26]. This paper adds to the literature by carefully computing the relic density of DM through a high-mixed mediator including the effects of hadronic final states; updating constraints in light of recent direct detection, LHC, and rare meson decay results; and discussing the implications for the simplest DM variations (e.g asymmetric, inelastic, scalar). We find that for heavier mediators $m_\phi > m_\chi$, DM annihilating directly into SM particles is ruled out for nearly all DM candidates under the most conservative assumptions regarding the DM-mediator couplings and mass ratios. We also find that when the mediator is lighter and the relic abundance is set by secluded annihilation $\chi\bar{\chi} \rightarrow \phi\phi$, the mediator-Higgs mixing is bounded from below by the DM thermalization requirement and there remains much viable parameter space. Finally, we identify a representative set of future direct detection and meson decay experiments to extend coverage to much of the remaining territory.

This paper is organized as follows: In Section II we com-

pute the DM relic density and discuss how to conservatively compare this target against different kinds of bounds; in Section III, we describe generic constraints and future experimental projections applicable to the entire parameter space; in Sections IV and V we specify to the regimes in which the mediator decays to the DM and SM respectively; In Section VI we discuss the unique features of the compressed region of parameter space in which $m_\chi < m_\phi < 2m_\chi$; in Section VII we outline how varying the assumptions about the DM candidate relative to our benchmark scenario (introduced above) changes the viable parameter space; finally in Section VIII we offer concluding remarks.

II. THERMAL RELIC COMPARISON

Direct Annihilation ($m_\chi < m_\phi$)

In the regime where the mediator is heavier than the DM, the annihilation can only proceed via direct annihilation to SM fermions through the s -channel.¹ To leading order, the annihilation rate for Dirac fermion annihilation into elementary fermions $\chi\bar{\chi} \rightarrow f\bar{f}$ is p -wave

$$\sigma v_{\text{rel.}}(\chi\bar{\chi} \rightarrow f\bar{f}) = \frac{g_\chi^2 g_f^2 m_\chi^2 v_{\text{rel.}}^2}{8\pi(m_\phi^2 - 4m_\chi^2)^2} \propto g_\chi^2 g_f^2 \left(\frac{m_\chi}{m_\phi}\right)^4 \frac{1}{m_\chi^2}, \quad (5)$$

where $v_{\text{rel.}}$ is the relative velocity between annihilating particles. Away from resonance at $m_\phi \sim 2m_\chi$ (and up to corrections of order m_χ^2/m_ϕ^2), for a fixed value of $g_\chi^2 g_f^2 (m_\chi/m_\phi)^4$, the annihilation rate is independent of the m_χ/m_ϕ ratio or the individual values of g_χ and g_f . From the parametric dependence in Eq. (5), it is convenient to define a dimensionless quantity

$$\kappa_f \equiv g_\chi^2 g_f^2 \left(\frac{m_\chi}{m_\phi}\right)^4 = g_\chi^2 \left(\frac{m_f}{v} \sin\theta\right)^2 \left(\frac{m_\chi}{m_\phi}\right)^4, \quad (6)$$

so that the annihilation rate $\chi\bar{\chi} \rightarrow \phi^* \rightarrow f\bar{f}$ is uniquely specified by the value of κ_f for a given value of m_χ . In the regime where annihilation is predominantly to electrons, achieving the observed relic abundance requires

$$\kappa_e \simeq 10^{-11} \left(\frac{0.1}{\Omega_\chi h^2}\right) \left(\frac{m_\chi}{10 \text{ MeV}}\right)^2. \quad (7)$$

Including all kinematically accessible channels and exploiting the mass proportionality of Higgs couplings, the full annihilation cross section can be written in terms of κ_e

$$\sigma v_{\text{rel.}}(\chi\bar{\chi} \rightarrow \text{SM}) \propto \frac{1}{m_\chi^2} \sum_f \kappa_f = \frac{\kappa_e}{m_\chi^2} \sum_f \left(\frac{m_f}{m_e}\right)^2, \quad (8)$$

¹ For an interesting counterexample see [17] where DM annihilates predominantly to pairs of heavier mediators (the so-called “forbidden” channel) by sampling the tail of the DM Boltzmann distribution at freeze out. For completeness, we also mention the possibility of $2 \rightarrow 3$ [27] and $3 \rightarrow 2$ annihilation [28] though the cases studied in these papers represent departures from the Higgs-mixing benchmarks considered in this paper

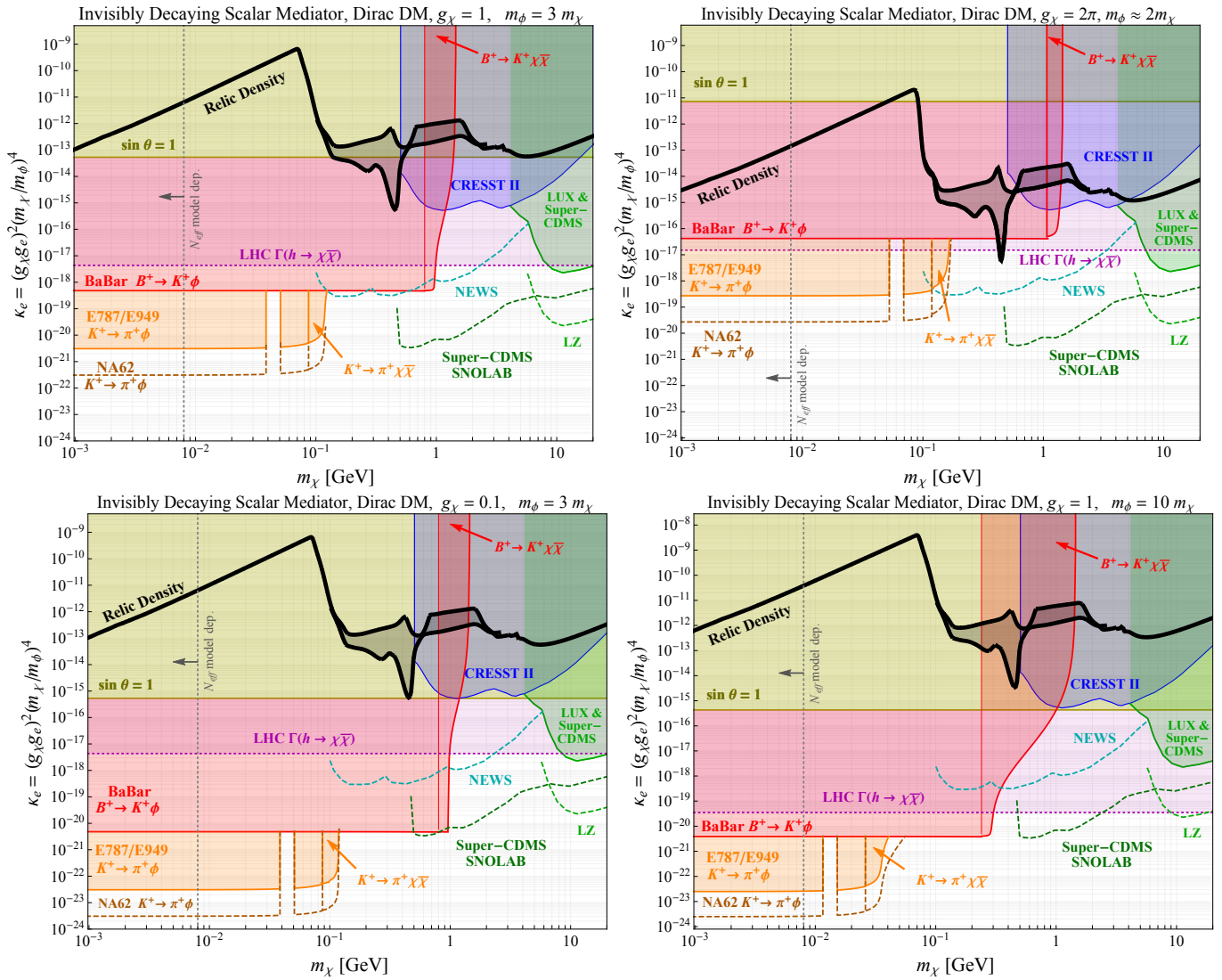


FIG. 2. Experimental constraints on Dirac fermion DM that annihilates through a light, Higgs-mixed mediator. We normalize the vertical axis using the e - ϕ coupling, g_e introduced in the text because this coupling always contributes to the annihilation over the mass range considered here—see discussion in Section II. **Top Left:** Parameter space for $m_\chi < m_\phi$ compared against the relic density contour computed assuming $m_\phi = 3m_\chi$ (solid black curve). The curve bifurcates near $m_\chi \sim m_\pi$ where there is disagreement in the literature about light Higgs couplings to hadronic states (see text). Like the relic density contour, the direct detection constraints are also invariant under different assumptions about the mass ratio and DM-mediator coupling since the SM-DM scattering cross section is proportional to the κ_e variable plotted on the vertical axis. However, for meson decay and collider constraints, which only constrain the mediator-Higgs mixing, we adopt the conservative values $g_\chi = 1$ and $m_\chi/m_\phi = 1/3$ for building $(g_\chi g_e)^2 (m_\chi/m_\phi)^4$ for comparison with the solid black relic curve; choosing smaller values of either quantity makes these constraints stronger—except in the resonant annihilation region. **Top Right:** Same as left, but in the resonant annihilation region $m_\phi \approx 2m_\chi$, which is the only regime in which the relic density curve moves appreciably. This plot also adopts the extreme value $g_\chi = 2\pi$ near the perturbativity limit, and reveals the maximum amount of viable parameter space for this scenario. As on the top-left plot, direct detection constraints and projections remain invariant, but the meson and collider bounds shift slightly as they are now computed for $m_\chi/m_\phi = 1/2.2$ instead. **Bottom Right:** Same as top-left, but with $m_\phi = 10m_\chi$. **Bottom Left:** Same as top-left, but with the reduced coupling $g_\chi = 0.1$.

which is applicable to all m_χ (MeV–GeV) considered in this paper, so we will present our direct annihilation results in terms of κ_e without loss of generality. For a more careful treatment of thermal freeze out, corresponding to the methodology in our numerical studies, see Appendix B.

For $m_\chi \gtrsim \Lambda_{\text{QCD}}$, the annihilation also proceeds through

several hadronic channels, whose interactions with the mediator are not simply-related to quark Yukawa couplings (e.g. $\chi\chi \rightarrow \pi^+\pi^-$). To account for these final states, we extract this coupling from simulations of hadronically-decaying light-

Higgs bosons [29] with the ansatz

$$g_f(s) \simeq \sin \theta \sqrt{\frac{8\pi}{m_h} \Gamma(h \rightarrow \text{SM})} \Big|_{m_h=\sqrt{s}}, \quad (9)$$

which is valid up to corrections of order m_f^2/s where s is the mandelstam variable ($s \approx 4m_\chi^2$ near freeze out). However, there are significant, order of magnitude discrepancies among the various computations of $\Gamma_h(h \rightarrow \text{hadrons})$ [30–35] (see Fig. 1 in [29]), so we regard this ansatz as reasonable in the interpolation region. We have checked that the couplings extracted using this approach recover the correct light Higgs width in the regions well above and below Λ_{QCD} .

The solid black lines shown in the panels of Fig. 2 represent the relic density contour computed precisely for different choices of mass and coupling ratios. These plots illustrate how, away from resonance, the parameter space for thermal freeze-out is invariant with respect to κ_e as a function of m_χ . The curves bifurcate near Λ_{QCD} to account for the different theoretical extractions of hadronic couplings in the region where annihilation is predominantly to hadrons; the upper and lower curves bracket the range of discrepant values from the literature [30–35].

In analogy with the s -channel annihilation process, the cross-section for non-relativistic DM-SM scattering in direct detection through ϕ exchange also has the same scaling $\sigma \propto \kappa_e/m_\chi^2$, up to order one corrections when the DM-nucleon masses are comparable. However, the constraints at most accelerator based experiments do not scale in this way; typically they only constrain the magnitude of a SM-mediator coupling and are insensitive to the mediator-DM coupling (and often also the masses of DM and mediator when the energy scale of the process is larger than the masses of dark sector states). For instance, the B and K decay bounds (See Sec IV) depend on the mass ratio since these bounds only constrain the mediator-SM coupling, so we have to choose a value of $g_\chi^2(m_\chi/m_\phi)^4$ to construct κ_e and plot these constraints against the thermal relic contour. For these bounds, choosing a very small g_χ or m_χ/m_ϕ ratio trivially covers arbitrarily small values of κ_e so the conservative choice is to take $g_\chi \sim m_\chi/m_\phi \sim \mathcal{O}(1)$ (see the caption in Fig. 2 and discussion below for more details).

On the upper-right panel of Fig. 2, we evaluate the same relic target, experimental bounds, and future projections for $m_\phi/m_\chi = 2.2$, which is very close to resonance, for which the relic target does move appreciably downwards relative to the relic density curves in other panels. In this panel we also adopt the extreme value $g_\chi = 2\pi$ near the perturbativity limit, for which this model requires a UV completion near the GeV scale. Nonetheless, even in this *extremely* conservative regime where the constraints are the weakest (all either shift upwards or are unaffected relative to the other panels) and thermal freeze requires the smallest κ_e values for the direct annihilation scenario, there is no viable territory left and the direct annihilation scenario is ruled out.² From the other plots in

Fig. 2, we see that the relic target for direct annihilation is decisively covered over the full MeV–GeV mass range.

Annihilation Into Mediators ($m_\chi > m_\phi$)

If the mediator is lighter than the DM, the direct annihilation is sharply suppressed relative to the t-channel process $\chi\chi \rightarrow \phi\phi$, which no longer scales as κ_e/m_χ^2 . Instead we have

$$\sigma_{v_{\text{rel}}}(\chi\chi \rightarrow \phi\phi) = \frac{3g_\chi^4 v_{\text{rel}}^2}{128\pi m_\chi^2}, \quad (10)$$

which is independent of the ϕ - h mixing angle, so thermal freeze out is compatible with a wide range of mixing angle values. However, for sufficiently small $\sin \theta$, the dark and visible sectors no longer thermalize, so there is a lower bound on the parameter space; for smaller mixing angles the abundance must be generated by a nonthermal mechanism, so this scenario is beyond the scope of this work.

III. GENERIC BOUNDS

CMB Although any viable thermal DM candidate is frozen out well before recombination, out of equilibrium annihilation around $z \sim 1100$ can still reionize hydrogen at the surface of last scattering and thereby modify the CMB power spectrum. The Planck constraint $\langle \sigma v \rangle_{\text{cmb}}/m_\chi \lesssim 3 \times 10^{-28} \text{ cm}^3 \text{ s}^{-1} \text{ GeV}^{-1}$ rules out thermal DM below 10 GeV [36] if the annihilation rate is s -wave (velocity independent). However, the annihilation rates for our benchmark scenarios in Eqs. (5) and (10) are p -wave so the annihilation rate is many orders of magnitude smaller on account of the velocity redshift from $T \sim m_\chi$ at freeze out and $T \sim \text{eV}$ at recombination. Thus neither of our annihilation topologies is constrained by CMB power injection.

Relativistic Degrees of Freedom If DM freezes out after neutrinos decouple, the annihilation byproducts can reheat photons relative to neutrinos, thereby decreasing the effective relativistic degrees of freedom, N_{eff} . [37]. At face value this excludes thermal DM below $\lesssim 10 \text{ MeV}$ (with order one variations depending on the particle identity of the DM). However, this bound is model dependent because the deficit in N_{eff} can be compensated for with additional hidden sector radiation or new physics in the neutrino sector.

Higgs Decays The ϕ - h mixing induces an invisible decay channel for the SM Higgs via $h \rightarrow \chi\chi$. Assuming only SM Higgs production mechanisms, the strongest limit on the invisible width arises from LHC measurements of $pp \rightarrow \text{jets} + \cancel{E}_T$, which can be interpreted to constrain the VBF production

² This conclusion depends somewhat on how large of a coupling a given

model can viably generate and on the theory uncertainty of the mediator-SM coupling near Λ_{QCD} , but aside from these caveats, the direct annihilation scenario is ruled out.

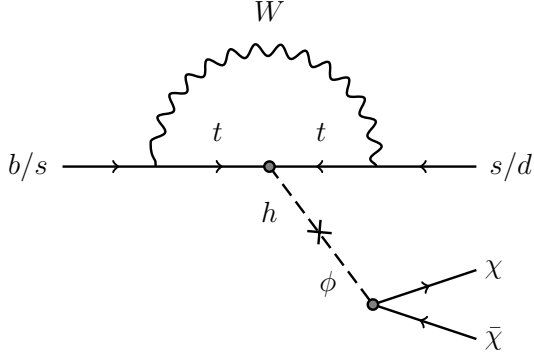


FIG. 3. Leading short distance contribution to $B^+ \rightarrow K^+ \chi \chi$ and $K^+ \rightarrow \pi^+ \bar{\chi} \chi$ decay due to scalar mediated interactions. For $m_\phi < m_B - m_K$, this decay can also proceed via $B^+ \rightarrow K^+ \phi$. Similar diagrams yield for ϕ mediated contributions to fully SM final states (e.g. $B^+ \rightarrow K^+ \mu^+ \mu^-$).

mechanism $pp \rightarrow \text{jets} + (h \rightarrow \chi \chi)$. A recent ATLAS measurement has extracted a limit of $\text{Br}(h \rightarrow \text{invisible}) < 0.3$ [38], which for our scenario implies

$$g_\chi^2 \sin^2 \theta \lesssim 4 \times 10^{-5}, \quad (11)$$

or in terms of the variable plotted in top left panel of Fig. 2, $\kappa_e \lesssim 7 \times 10^{-18}$, where the mass ratio is conservatively taken to be $m_\chi/m_\phi = 1/3$; heavier mediators make this constraint more severe, so this choice reveals the available gaps subject to the condition that the mediator decays invisibly and that $\chi \chi \rightarrow ff$ annihilation is off resonance.

In addition to the mixing, the mixed $\phi - h$ quartic interaction may also contribute to exotic Higgs decays via $h \rightarrow \phi \phi$ [39]. If ϕ decays invisibly to DM, this process contributes to the Higgs invisible width, and if ϕ decays visibly the process can induce an array of SM final states, which reconstruct the Higgs invariant mass and yield nested internal resonances. However, the bounds and prospects for both scenarios depend exclusively on the size of the quartic which does not affect the DM thermal history or the bounds presented in this paper, so a proper treatment of this possibility is beyond the scope of the present work.

We also note that there are additional constraints on the mixing angle $\sin \theta$ from rare $h \rightarrow \phi \phi$ decays. However, the branching ratio for this process depends on a different diagrams which are sensitive to the mixing angle, mixed $h^2 \phi^2$ quartic coupling, and the ϕ^3 cubic coupling, so the precise bound arising from this process is model dependent and cannot be presented in Fig. 2 without additional assumptions about these other parameters.

IV. INVISIBLY DECAYING MEDIATOR ($m_\phi > 2m_\chi$)

Rare Meson Decays If ϕ decays invisibly, this scenario induces rare meson decays $B^+ \rightarrow K^+ \phi$ and is constrained by limits on the $B^+ \rightarrow K^+ \nu \bar{\nu}$ branching fraction. The loop

level process arises from the effective Higgs mixing interaction [20, 22]

$$\mathcal{L}_{\text{FCNC}} \supset (C_{sb} \bar{s}_L b_R + C_{sd} \bar{s}_L d_R) \phi, \quad (12)$$

where $C_{sb, sd}$ are effective coefficients that induce flavor changing processes.

B-Meson Decays For B-mesons, The effective coefficient of interest is

$$C_{sb} = \frac{3g_W^2 m_b m_t^2 V_{ts}^* V_{tb} \sin \theta}{64\pi^2 m_W^2 v} = 6.4 \times 10^{-6} \sin \theta, \quad (13)$$

and this interaction has the partial width [40]

$$\Gamma_{B \rightarrow K \phi} = \frac{|C_{sb}|^2 f_0(m_\phi)^2 (m_{B^+}^2 - m_K^2)^2}{16\pi m_{B^+}^3} \xi(m_B, m_K, m_\phi), \quad (14)$$

$$\xi(a, b, c) = \sqrt{(a^2 - b^2 - c^2)^2 - 4b^2 c^2}, \quad (15)$$

where the scalar form factor can be parametrized $f_0(q) = 0.33(1 - q^2/38 \text{ GeV}^2)^{-1}$ [41]. The total B-meson width is $\Gamma_{B^+} = 4.1 \times 10^{-13} \text{ GeV}$ [42], so the branching ratio has the approximate scaling

$$\text{Br}(B^+ \rightarrow K^+ \phi) \sim \frac{|C_{sb}|^2 f_0(m_\phi)^2 m_{B^+}^3}{16\pi m_b^2 \Gamma_{B^+}} \approx 1.5 \sin^2 \theta, \quad (16)$$

which, for our conservative benchmark inputs $g_\chi = 1$ and $m_\chi = 3m_\phi$, the BaBar limit $\text{Br}(B^+ \rightarrow K^+ \nu \bar{\nu}) < 1.6 \times 10^{-5}$ [43] requires

$$\kappa_e = (g_\chi g_e)^2 \left(\frac{m_\chi}{m_\phi} \right)^4 \lesssim 5.6 \times 10^{-19}. \quad (17)$$

The exact bound for this DM/mediator mass ratio shown in Fig. 2 (left) is computed from Eq. (14) using the efficiencies used in [43] is slightly stronger because the two-body $B^+ \rightarrow K^+ \phi$ process has greater kinematic acceptance relative to $B^+ \rightarrow K^+ \nu \bar{\nu}$.

Kaon Decays An invisibly decaying light scalar can also yield $K \rightarrow \pi \phi$ decays for which the partial width is

$$\Gamma_{K^+ \rightarrow \pi^+ \phi} = \frac{|C_{ds}|^2 (m_{K^+}^2 - m_{\pi^+}^2)^2}{16\pi m_K^3} \xi(m_K, m_\pi, m_\phi), \quad (18)$$

Unlike in Eq. (14), the analogous scalar form factor is close to unity [44] and can be neglected. The effective FCNC coefficient from Eq. (12) is

$$C_{sd} = \frac{3g_W^2 m_s m_t^2 V_{ts}^* V_{td} \sin \theta}{64\pi^2 m_W^2 v} = 1.2 \times 10^{-9} \sin \theta, \quad (19)$$

The total Kaon width is $\Gamma_{K^+} = 5.3 \times 10^{-17} \text{ GeV}$, so the branching ratio is approximately

$$\text{Br}(K^+ \rightarrow \pi^+ \phi) \sim \frac{|C_{sd}|^2 m_{K^+}^3}{16\pi m_s^2 \Gamma_{K^+}} \approx 6.7 \times 10^{-3} \sin^2 \theta, \quad (20)$$

This final state contributes to the E797 and E949 measurements of $\text{Br}(K^+ \rightarrow \pi^+ \nu \bar{\nu}) = (1.73_{-1.05}^{+1.15}) \times 10^{-10}$ [45]. To

avoid an order one correction to we demand $\sin^2\theta \lesssim 2.5 \times 10^{-8}$, which, for our benchmarks $g_\chi = 1$ and $m_\phi = 3m_\chi$ implies

$$\kappa_e = (g_e g_\chi)^2 \left(\frac{m_\chi}{m_\phi} \right)^4 \lesssim 1.4 \times 10^{-21}. \quad (21)$$

The exact bound computed using Eq. (18) and the efficiencies in [45] is presented as the orange regions of Fig. 2; the sensitivity gap near m_χ corresponds to an experimental cut on final-state pion momentum. Also shown in Fig. 2 is the projected sensitivity of NA62 [46] assuming $10^{13} K^+$ and sensitivity for a 10 % measurement of the $K^+ \rightarrow \pi^+ \nu \bar{\nu}$ branching ratio with identical cuts and efficiencies as [45].

Direct Detection For light, non-relativistic DM with $v \sim 10^{-3}$, scattering off nuclei yields recoil energies that fall below experimental thresholds. However, electron scattering results from XENON10 and future results can constrain this parameter space [47, 48]. At Xenon 10 the non relativistic, spin-independent cross section for scattering off nucleon (N) at direct detection experiments is

$$\sigma_{\chi N} = \frac{|C_{\phi N}|^2 g_\chi^2 \mu_{\chi N}^2}{\pi m_\phi^4}, \quad (22)$$

where $\mu_{\chi N}$ is the DM-nucleon reduced mass and the effective ϕ coupling to nucleons can be written [49]

$$C_{\phi N} = \frac{\sqrt{2} \sin \theta m_N}{v} \left(\frac{6}{27} f_{TG}^{(N)} + \sum_{q=u,d,s} f_{Tq}^{(N)} \right), \quad (23)$$

where $f_{TG}^{(N)}, f_{Tq}^{(N)} \sim \mathcal{O}(0.1)$ are determined by averaging the entries in the Appendix of [50]. In Fig. 2 we present the direct detection limits for the invisibly decaying case $m_\phi > 2m_\chi$ in terms of the parameter combination responsible for thermal freezeout.

$$\sigma_{\chi N} \sim 0.1 \frac{m_N^2}{m_e^2} \frac{\mu_{\chi N}^2}{\pi m_\phi^4} \times (g_\chi g_e)^2 \left(\frac{m_\chi}{m_\phi} \right)^4, \quad (24)$$

which, for a fixed cross section yields an estimated

$$\kappa_e = (g_\chi g_e)^2 \left(\frac{m_\chi}{m_\phi} \right)^4 \sim 10^{-15} \left(\frac{10^{-38} \text{ cm}^2}{\sigma_{\chi N}} \right) \left(\frac{m_\chi}{\text{GeV}} \right)^2. \quad (25)$$

For each m_χ there is a unique value of κ_e constrained by direct detection, so these curves are invariant under different assumptions about the individual ratios that constitute this variable. Using this notation in Figs. 2 we present direct detection limits from LUX [51] Super-CDMS [52], and new results from CRESST-II [53], which combine to rule out the thermal relic curve. We also show projections for upcoming and planned experiments NEWS [54] and Super-CDMS SNO-LAB [55], and LZ [55]

V. VISIBLY DECAYING MEDIATOR ($m_\phi < 2m_\chi$)

When the mediator is lighter than the DM, the annihilation rate for freeze out is decoupled from the mixing angle

and there is no clear target of opportunity for decisive experimental coverage; the observed abundance is compatible with a wide range of mixing angles. Nonetheless, there is still a lower bound on the SM-DM interaction from the requirement that the DM thermalize in the early universe.

Thermal Equilibrium For sufficiently weakly coupled mediators, the DM never achieves thermal equilibrium with the visible sector radiation, so there is no model-independent minimum annihilation rate required to avoid overclosure. Unlike in the direct annihilation scenario (where $m_\chi < m_\phi$), the thermalization criterion now applies to the mediator since the relic abundance is set by $\chi\chi \rightarrow \phi\phi$ annihilation, so the DM is always in thermal contact with the mediator. As in the former scenario, we determine the requisite $\sin \theta$ by solving $n_t(T) \langle \sigma v \rangle \sim H(T)$ near $T \sim m_t$, which yields the approximate requirement

$$g_\chi^2 \sin^2 \theta \gtrsim \frac{53\pi^3 \sqrt{g_*(m_t)} m_t}{\zeta(3) m_{Pl}} \approx 2 \times 10^{-13}, \quad (26)$$

which defines the gray shaded region in Fig. 3. Note that this bound is insensitive to the DM and mediator masses below the electroweak scale. Here we have taken $n_t \propto m_t^3$. For a more thorough treatment of thermalization, see the discussion in Appendix C.

Beam-Dumps The CHARM Collaboration placed direct limits on light axion-like particles using a 400 GeV proton beam impinging on a copper target [56]. In Fig. 4 we show the constraint computed in [29] (see also [23, 57] for similar results) in the yellow shaded region. We also show projections for an analogous beam dump search using the SHiP facility at CERN (dashed brown contour) [57].

Visible Meson Decays A visibly decaying scalar mediator can contribute to the process $B^+ \rightarrow K^+ \mu^+ \mu^-$, which is tightly constrained by LHCb and Belle measurements of the branching ratio. In Fig. 3 we show the constraint on the $\phi - h$ mixing angle as a function of light mediator mass as computed in [23, 29]. The gaps in the coverage near $m_\phi \sim 2 - 3 \text{ GeV}$ are regions vetoed by the search criteria in [58, 59]. In the same parameter space, we also show bounds from measurements of the $K_L \rightarrow \pi^0 \ell^+ \ell^-$ branching ratio [60, 61] as extracted in [57] for light scalars using the analysis to bound pseudoscalar mediators in [40].

BBN A sufficiently light ($m_\phi \lesssim 10 \text{ MeV}$), weakly coupled scalar particle with a thermal number density can decay appreciably during Big Bang Nucleosynthesis (BBN) and spoil the successful predictions of light element yields accumulated in the early universe. To leading order, the partial widths for SM decay channels are [62]

$$\Gamma(\phi \rightarrow f\bar{f}) = s^2 \theta \frac{G_F m_f^2 m_\phi}{4\sqrt{2}} \left(1 - \frac{4m_\chi^2}{m_\phi^2} \right)^{3/2}, \quad (27)$$

$$\Gamma(\phi \rightarrow \gamma\gamma) = s^2 \theta \frac{G_F \alpha^2 m_\phi^3}{128\sqrt{2}\pi^3} \left| \sum_f N_c Q_f^2 A_{1/2}(\tau_f) + A_1(\tau) \right|^2, \quad (28)$$

$$\Gamma(\phi \rightarrow gg) = s^2 \theta \frac{G_F \alpha_s^2 (m_\phi) m_\phi^3}{36\sqrt{2}\pi^3} \left| \frac{3}{4} \sum_q A_{1/2}(\tau_q) \right|^2, \quad (29)$$

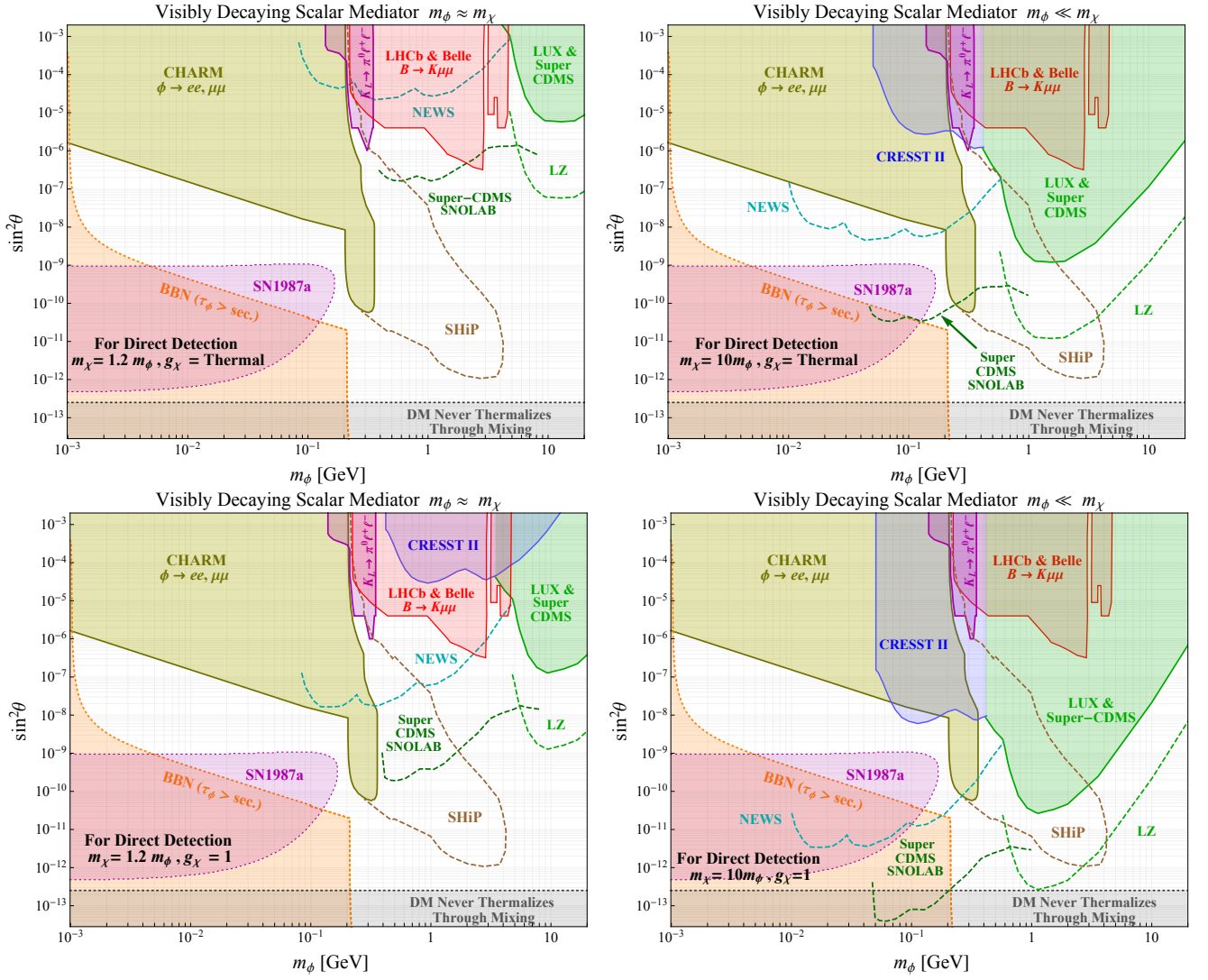


FIG. 4. Existing constraints on the mediator-Higgs mixing in the visibly decaying $\phi \rightarrow \text{SM SM}$ regime. **Top row:** The DM is a particle-antiparticle symmetric thermal relic whose abundance is set by t -channel $\chi\chi \rightarrow \phi\phi$ annihilation, which determines the requisite g_χ coupling for a given DM mass point. Note that most of the parameter space is covered by direct searches for the mediator decaying into SM particles, so except for direct detection, the plots do not require any assumption about the DM provided that the mediator decays visibly. For direct detection, we show two different regimes: $m_\chi \approx m_\phi$ (but with a slightly lighter mediator) which is the least constrained regime, and $m_\chi = 10 m_\phi$; for $m_\chi/m_\phi > 10$, the DM is no longer light in this parameter space, so this regime is beyond the scope of this work. **Bottom row:** Same as top row, but with $g_\chi = 1$, which corresponds to couplings larger than thermal, but still compatible with asymmetric DM, whose antiparticles have all been depleted by annihilation; these plots represent the most aggressive bounds and projections compatible with both DM-SM equilibration and perturbative unitarity. Combined, these four plots bracket the full parameter space of interest; smaller mass ratios than shown on the left column would invalidate the visibly decaying assumption; larger mass ratios than the right column would no longer correspond to the light DM regime; smaller DM-mediator couplings than the top row would overclose the universe; larger DM-mediator couplings than the bottom row would require a UV completion near the GeV scale. Note also that the plots in the left column show bounds from N_{eff} (gray vertical dashed curves) [37] due to light DM freeze-out after neutrino decoupling (see text); the right column does not show this bound because for $m_\chi \sim 10m_\phi$ the left boundary of these plots, corresponding to $m_\chi \sim 10$ MeV, is safe from this constraint.

where $\tau_i \equiv m_\phi^2/4m_i^2$, N_c is the number of colors for a given fermion species, Q_f is its electromagnetic charge, $s^2\theta \equiv \sin^2\theta$ and

$$A_{1/2}(\tau) = 2[\tau + (\tau - 1)f(\tau)]\tau^{-2}, \quad (30)$$

$$A_1(\tau) = -[2\tau^2 + 3\tau + 3(2\tau - 1)f(\tau)]\tau^{-2}, \quad (31)$$

where the function $f(\tau)$ satisfies

$$f(\tau) = \begin{cases} \arcsin^2 \sqrt{\tau} & \tau \leq 1 \\ -\frac{1}{4} \left[\log \frac{1+\sqrt{1-\tau^{-1}}}{1-\sqrt{1-\tau^{-1}}} - i\pi \right]^2 & \tau > 1, \end{cases} \quad (32)$$

and only kinematically accessible decay channels are included for a given m_ϕ ; in our numerical results we only include the

decay to gluons for $m_\phi > 2m_\pi$. Below the QCD confinement scale, we include hadronic decays following the prescription in Eq. (9). While a thorough treatment of the BBN constraint is beyond the scope of this paper, we safely demand that the lifetime satisfy $\Gamma_\phi^{-1} \lesssim 1$ sec, and show this boundary as the orange region in Fig. 3, which only covers thermal parameter space for masses where ϕ decays to e^+e^- and $\gamma\gamma$.

Since DM near the lower end of our mass range (\sim few MeV) freezes out during the epoch of BBN, in principle there is an additional constraint from the observed light element yields from this process as well. However, near freeze out, the DM number density is approximately

$$n_\chi \sim \frac{\Omega_\chi}{\Omega_b} \frac{m_p}{m_\chi} n_b = \frac{\Omega_\chi}{\Omega_b} \frac{m_p}{m_\chi} \eta n_\gamma, \quad (33)$$

where $\eta \equiv n_b/n_\gamma \sim 10^{-9}$ is the baryon to photon ratio, so even on the lower end of our mass range, $n_\chi \ll n_\gamma$ during BBN. Thus, DM annihilation products predominantly thermalize with SM photons before affecting the yields of any nuclear species during BBN.

Supernovae A light, weakly coupled scalar mediator can be produced on shell during a supernova (SN) explosion and significantly contribute to its energy loss, thereby shortening the duration of the observable neutrino pulse emitted during core collapse. The most significant such constraint arises from SN1987a which has been used to constrain the parameter space for axions and axion-like particles [63–66] whose SN production is dominated by radiative production off nucleons. Following the prescription in [67], the energy loss rate per unit volume due to ϕ production is

$$Q_\phi \sim C_{\phi N}^2 \frac{11}{(15\pi)^3} \left(\frac{T}{m_\pi}\right)^4 p_F^5 G_\phi \left(\frac{m_\pi}{p_F}\right) \xi(T, m_\phi), \quad (34)$$

where $p_F \sim 200$ MeV is the SN Fermi momentum, the function G_ϕ satisfies [67]

$$G_\phi(u) = 1 - \frac{5}{2}u^2 - \frac{35}{22}u^4 + \frac{5}{64}(28u^3 + 5u^5) \tan^{-1}\left(\frac{2}{u}\right) + \frac{5}{64} \frac{\sqrt{2}u^6}{\sqrt{2+u^2}} \tan^{-1}\left(\frac{2\sqrt{2(u^2+2)}}{u^2}\right), \quad (35)$$

and we have appended the additional factor

$$\xi(T, m_\phi) \equiv \frac{\int_{m_\phi}^{\infty} dx \frac{x \sqrt{x^2 - m_\phi^2}}{e^{x/T} - 1}}{\int_0^{\infty} dx \frac{x^2}{e^{x/T} - 1}}, \quad (36)$$

to approximately account for the finite scalar mass effects, which were not included in [67]. To extract an approximate bound from SN1987a, we demand that the total energy-loss rate satisfy $P_{\text{esc.}} Q_\phi V_{\text{SN}} \lesssim 10^{53}$ erg/s where $V_{\text{SN}} = (4\pi/3)R_{\text{SN}}^3$ is the SN volume, $R_{\text{SN}} = 10$ km is its radius, and

$$P_{\text{esc.}} = \exp(-R_{\text{SN}}/\gamma c\tau_\phi) \exp(-R_{\text{SN}}/\lambda_\phi), \quad (37)$$

is the probability that ϕ escapes without decaying or being reabsorbed within the supernova interior, where $\gamma\tau_\phi$ is the average boosted lifetime and λ_ϕ its the mean free path. Following [63], we estimate the latter using detailed balance

$\lambda_\phi^{-1} \sim Q_\phi/\rho_\phi$ where ρ_ϕ is the scalar energy density estimated in the equilibrium limit for $T_{\text{SN}} \sim 30$ MeV.

In Fig. 4 we show the excluded region shaded in purple and labeled SN1987a. Since this estimate is only valid at the order of magnitude level, the region is plotted with a dotted boundary; given the exponential sensitivity to some aspects of this treatment, a dedicated study is required to extract a more rigorous bound, but is beyond the scope of this work.

Direct Detection For a visibly decaying mediator, the physics of direct detection is identical to that of the invisible case considered above. However, since we are now interested in the $\sin^2\theta$ vs. m_ϕ parameter space, we have to make an assumption about the DM mass in order to plot the direct detection bound on the same plane in Fig. 4; all other constraints in this parameter space depend only on the mixing and the mediator mass. Nonetheless, we can still comprehensively capture the parameter space compatible with light, thermal DM ($<$ few GeV) by looking at the two extreme choices of mass ratios: $m_\chi = 1.2m_\phi$ (Fig. 3, left column) and $m_\chi = 10m_\phi$ (Fig. 3, right column) for much smaller ratios, the mediator starts to decay visibly and for much larger ratios the DM is no longer “light”. In addition to specifying the DM-mediator mass ratio, we must also choose g_χ to extract a limit on $\sin\theta$. For the top row of Fig. 3, our choice (for a fixed DM-mediator mass ratio) we choose g_χ to yield the observed relic abundance through symmetric thermal freeze out via $\chi\bar{\chi} \rightarrow \phi\phi$; this is the most conservative choice as it corresponds to the smallest coupling consistent with thermal relic DM and correspondingly yields the weakest direct detection constraints and future projections. For the lower row in Fig. 4 we consider the opposite regime $g_\chi = 1$ which is near the unitarity boundary and (if χ constitutes all the DM) is compatible with asymmetric DM scenario in which the larger-than-thermal annihilation rate efficiently depletes most of the dark antiparticles produced in thermal equilibrium with the visible sector

VI. VISIBLY DECAYING MEDIATOR, COMPRESSED REGIME ($m_\chi < m_\phi < 2m_\chi$)

In the compressed region of parameter space where $m_\chi < m_\phi < 2m_\chi$, DM annihilation proceeds through an off-shell ϕ via $\chi\chi \rightarrow \phi^* \rightarrow ff$, which depends on κ_e as described in Sec. II. Furthermore, since $m_\chi/m_\phi \sim 1$, we have

$$\kappa_e = (g_\chi g_e)^2 \left(\frac{m_\chi}{m_\phi}\right)^4 \approx g_\chi^2 \left(\frac{m_e}{v} \sin\theta\right)^2 = 4.3 \times 10^{-12} g_\chi^2 \sin^2\theta, \quad (38)$$

but from Eq. (7), thermal freeze out in the light DM mass range requires $\kappa_e \sim 10^{-13} (m_\chi/\text{MeV})^2$, so the requisite mixing angle must be $\sim \mathcal{O}(1)$ for a sufficiently large annihilation rate. However, unlike the regime considered in Sec. IV, for the $m_\phi < 2m_\chi$ mass range, the mediator only decays to SM fermions, so all the constraints from Sec.V are applicable. From Fig. 4, it is clear that, so long as ϕ decays visibly, the region $\sin^2\theta \gtrsim 10^{-5}$ is excluded over the full MeV-GeV

mass range. Thus, we conclude that this compressed region of parameter space is ruled out for thermal DM.

VII. DARK MATTER CANDIDATE VARIATIONS

We now consider simple variations away from the particle-antiparticle symmetric Dirac fermion DM candidate from the benchmark model in Eqs. (3) and (4). In short, we find that for scenarios involving Majorana DM, scalar DM, asymmetric DM, or fermion DM with parity odd couplings, the analogous parameter space is either qualitatively unchanged or more severely constrained relative to the symmetric Dirac scenario with parity even interactions. The following analysis, therefore, justifies our choice of benchmark model as sufficiently representative of the remaining viable parameter space.

Parity Odd Couplings In the Lagrangian for our benchmark scenario, Eq. (3), allows a $\phi\bar{\psi}\gamma^5\psi$ term. This interaction gives rise to s wave annihilation for both $\chi\bar{\chi} \rightarrow f\bar{f}$ and $\chi\bar{\chi} \rightarrow \phi\phi$ channels, which is robustly ruled out for thermal relic DM below $\lesssim 10$ GeV (see Sec. III), so at minimum, we require $g'_\chi \ll g_\chi$. Although in principle, we could keep this subdominant in our analysis, its presence would not significantly change the qualitative character of any plots; it would only introduce percent level corrections for couplings that evade CMB bounds, so we have not lost any essential generality by setting $g'_\chi = 0$ in the analysis presented above.

Majorana DM The simplest variation on our benchmark scenario involves exchanging our Dirac DM with a Majorana fermion. However, most of the constraints we encounter below involve accelerator production, meson decays, or direct detection; none of which differs substantially with this modification. Thus, the constraints and relic density projections will differ only by order one amounts.

Scalar Symmetric DM If the DM, itself, is a stable scalar φ that couples to the Higgs-portal mediator ϕ , the relic abundance can be achieved through either direct annihilation $\varphi\varphi \rightarrow \phi^* \rightarrow f\bar{f}$ ($m_\varphi > m_\phi$) or t-channel $\varphi\varphi \rightarrow \phi\phi$ ($m_\varphi > m_\phi$) annihilation. In both cases, the leading annihilation rates will be s -wave (velocity independent) and, therefore, ruled out by CMB power-injection limits for φ masses below 10 GeV [36].

Asymmetric DM If the dark matter abundance is set by a primordial asymmetry [68–72] and the dark matter achieves thermal equilibrium with the SM, the annihilation rate must be larger than the nominal freeze out value [73, 74]. However, all other constraints on its direct production and detection remain identical; since antiparticles are exponentially depleted below $T \lesssim m_{\text{DM}}$, the indirect detection signatures are generically suppressed at late times, so asymmetric DM can be compatible with the CMB. Thus, the results in this paper apply fully well to this variation, but the parameter space compatible with the observed abundance (for the direct annihilation topology $m_\chi < m_\phi$) is above the solid black curve in Fig. 2 (see discussion below), so this is also ruled out; for particle-antiparticle symmetric scalar DM, which has an s -wave annihilation rate,

the relic density contour will shift slightly lower in the parameter space by an $\mathcal{O}(1)$ amount, but everything else remains quantitatively similar.

Inelastically Coupled DM In principle, an extended dark sector can couple inelastically to the mediator ϕ , which can sharply suppress direct detection limits. A full treatment of this scenario is beyond the scope of this work, but we note that a minimal DM model can not easily ensure that the singlet scalar couple predominantly inelastically to either SM or DM fields. The simplest such mechanism in the case of a vector mediator involves a pseudo-Dirac splitting of Weyl fermions with both Dirac and Majorana masses [75], which yields a predominantly inelastic coupling in the mass eigenbasis and yields distinctive direct detection and collider phenomenology [76, 77]. However, for a scalar mediator, the analogous procedure yields comparable elastic and inelastic contributions, so the scenario is qualitatively similar to the benchmark model we consider throughout this paper; all of the same bounds will apply, but there will be order one variations from the existence of additional couplings.

VIII. CONCLUDING REMARKS

In this paper we have mapped out parameter space for light ($< \text{few GeV}$) thermal DM coupled to a light scalar that mixes with the SM Higgs boson. Although we have focused primarily on a benchmark model with a Dirac fermion DM candidate, this scenario suffices to capture most of the essential physics, so our central conclusions apply to the simplest DM variations (e.g. asymmetric DM or scalar DM with the same mediator).

In the more predictive, heavier-mediator regime ($m_\phi > m_\chi$) we find that thermal DM is now conservatively ruled out by a combination of rare meson decay, direct detection, and off-shell Higgs width measurements. This conclusion holds regardless of the DM/mediator mass ratio so long as the latter is heavier. We also find that benchmark future low-threshold direct detection experiments (NEWS, Super-CRDS, SNOLAB, LZ and others) can improve coverage for the Higgs portal interaction, but (since the thermal relic parameter space is ruled out) this improvement would only test a subdominant interaction in the dark sector – additional interactions would be required to avoid overclosure.

Relaxing the requirement that the light scalar mediator mix exclusively with the SM Higgs doublet, it may be possible to engineer a viable direct-annihilation scenario in a type-III two Higgs doublet model in which one doublet couples to quarks and the other couples to leptons. If the light scalar mixes predominantly with the leptonic doublet, it may be possible to relax the constraints from rare meson decays, but we leave this investigation for future work.

For the lighter mediator regime ($m_\phi > m_\chi$) in which DM annihilation proceeds through the “secluded” channel $\chi\chi \rightarrow \phi\phi$, there is no clear relic density target since the rate is

independent of the Higgs-mediator mixing; thermal freeze out is compatible with a wide range of SM-mediator couplings. However, the mixing angle is bounded from below by the requirement that the DM be produced thermally in the early universe and much of the parameter space (with notable gaps) is covered by a combination beam dump, supernovae, and BBN constraints below mediator masses of ~ 100 MeV. Above this range, there are additional constraints from direct detection experiments, which are poised to improve with the next generation of efforts, but the amount of new coverage will depend greatly on the DM/mediator mass ratio.

Finally, for the “compressed” regime ($m_\chi < m_\phi < 2m_\chi$) in which DM and mediator masses are nearly degenerate, DM annihilation proceeds via $\chi\chi \rightarrow \phi^* \rightarrow ff$, so there is a

thermal freeze out requirement on the Higgs- ϕ mixing angle. However, in this mass range, the mediator decays to visible SM states, so all the bounds from the $m_\phi > m_\chi$ mass range apply equally well and rule out the range of Higgs- ϕ mixings required for thermal freeze out.

Acknowledgments: We thank Wolfgang Altmanshoffer, Jackson Clarke, Roni Harnik, Eder Izaguirre, Maxim Pospelov, David Pinner, Kai Schmidt-Hoberg, Philip Schuster, Brian Shuve, Flip Tanedo, Jesse Thaler, and Natalia Toro for many helpful conversations. We also thank the University of Victoria for hospitality while this work was being completed. Fermilab is operated by Fermi Research Alliance, LLC, under Contract No. DE-AC02-07CH11359 with the US Department of Energy.

-
- [1] B. W. Lee and S. Weinberg, Phys.Rev.Lett. **39**, 165 (1977).
 - [2] B. Shakya, (2015), arXiv:1512.02751 [hep-ph].
 - [3] E. Izaguirre, G. Krnjaic, P. Schuster, and N. Toro, Phys. Rev. Lett. **115**, 251301 (2015), arXiv:1505.00011 [hep-ph].
 - [4] R. Essig, J. A. Jaros, W. Wester, P. H. Adrian, S. Andreas, *et al.*, (2013), arXiv:1311.0029 [hep-ph].
 - [5] R. Essig, P. Schuster, N. Toro, and B. Wojtsekhowski, JHEP **1102**, 009 (2011), arXiv:1001.2557 [hep-ph].
 - [6] H. Merkel *et al.* (A1 Collaboration), Phys.Rev.Lett. **106**, 251802 (2011), arXiv:1101.4091 [nucl-ex].
 - [7] S. Abrahamyan *et al.* (APEX Collaboration), Phys.Rev.Lett. **107**, 191804 (2011), arXiv:1108.2750 [hep-ex].
 - [8] E. Izaguirre, G. Krnjaic, P. Schuster, and N. Toro, Phys. Rev. **D88**, 114015 (2013), arXiv:1307.6554 [hep-ph].
 - [9] R. Dharmapalan *et al.* (MiniBooNE), (2012), arXiv:1211.2258 [hep-ex].
 - [10] E. Izaguirre, G. Krnjaic, and M. Pospelov, Phys. Rev. **D92**, 095014 (2015), arXiv:1507.02681 [hep-ph].
 - [11] E. Izaguirre, G. Krnjaic, P. Schuster, and N. Toro, (2014), arXiv:1411.1404 [hep-ph].
 - [12] B. Batell, R. Essig, and Z. Surujon, Phys.Rev.Lett. **113**, 171802 (2014), arXiv:1406.2698 [hep-ph].
 - [13] Y. Kahn, G. Krnjaic, J. Thaler, and M. Toups, (2014), arXiv:1411.1055 [hep-ph].
 - [14] M. Battaglieri *et al.* (BDX Collaboration), (2014), arXiv:1406.3028 [physics.ins-det].
 - [15] Y. Hochberg, Y. Zhao, and K. M. Zurek, (2015), arXiv:1504.07237 [hep-ph].
 - [16] D. Curtin, R. Essig, S. Gori, and J. Shelton, JHEP **02**, 157 (2015), arXiv:1412.0018 [hep-ph].
 - [17] R. T. D’Agnolo and J. T. Ruderman, Phys. Rev. Lett. **115**, 061301 (2015), arXiv:1505.07107 [hep-ph].
 - [18] C. P. Burgess, M. Pospelov, and T. ter Veldhuis, Nucl. Phys. **B619**, 709 (2001), arXiv:hep-ph/0011335 [hep-ph].
 - [19] M. Pospelov and A. Ritz, Phys. Rev. **D84**, 113001 (2011), arXiv:1109.4872 [hep-ph].
 - [20] C. Bird, R. V. Kowalewski, and M. Pospelov, Mod. Phys. Lett. **A21**, 457 (2006), arXiv:hep-ph/0601090 [hep-ph].
 - [21] M. Pospelov, A. Ritz, and M. B. Voloshin, Phys. Lett. **B662**, 53 (2008), arXiv:0711.4866 [hep-ph].
 - [22] C. Bird, P. Jackson, R. V. Kowalewski, and M. Pospelov, Phys. Rev. Lett. **93**, 201803 (2004), arXiv:hep-ph/0401195 [hep-ph].
 - [23] K. Schmidt-Hoberg, F. Staub, and M. W. Winkler, Phys. Lett. **B727**, 506 (2013), arXiv:1310.6752 [hep-ph].
 - [24] F. Piazza and M. Pospelov, Phys. Rev. **D82**, 043533 (2010), arXiv:1003.2313 [hep-ph].
 - [25] C. Kouvaris, I. M. Shoemaker, and K. Tuominen, Phys. Rev. **D91**, 043519 (2015), arXiv:1411.3730 [hep-ph].
 - [26] K. Kainulainen, K. Tuominen, and V. Vaskonen, (2015), arXiv:1507.04931 [hep-ph].
 - [27] A. Rajaraman, J. Smolinsky, and P. Tanedo, (2015), arXiv:1503.05919 [hep-ph].
 - [28] Y. Hochberg, E. Kuflik, T. Volansky, and J. G. Wacker, Phys. Rev. Lett. **113**, 171301 (2014), arXiv:1402.5143 [hep-ph].
 - [29] J. D. Clarke, R. Foot, and R. R. Volkas, JHEP **02**, 123 (2014), arXiv:1310.8042 [hep-ph].
 - [30] J. F. Gunion, H. E. Haber, G. L. Kane, and S. Dawson, Front. Phys. **80**, 1 (2000).
 - [31] M. B. Voloshin, Sov. J. Nucl. Phys. **44**, 478 (1986), [Yad. Fiz.44,738(1986)].
 - [32] B. Grinstein, L. J. Hall, and L. Randall, Phys. Lett. **B211**, 363 (1988).
 - [33] S. Raby and G. B. West, Phys. Rev. **D38**, 3488 (1988).
 - [34] J. F. Donoghue, J. Gasser, and H. Leutwyler, Nucl. Phys. **B343**, 341 (1990).
 - [35] T. N. Truong and R. S. Willey, Phys. Rev. **D40**, 3635 (1989).
 - [36] P. A. R. Ade *et al.* (Planck), (2015), arXiv:1502.01589 [astro-ph.CO].
 - [37] K. M. Nollett and G. Steigman, Phys. Rev. **D89**, 083508 (2014), arXiv:1312.5725 [astro-ph.CO].
 - [38] G. Aad *et al.* (ATLAS), JHEP **01**, 172 (2016), arXiv:1508.07869 [hep-ex].
 - [39] D. Curtin *et al.*, Phys. Rev. **D90**, 075004 (2014), arXiv:1312.4992 [hep-ph].
 - [40] M. J. Dolan, C. McCabe, F. Kahlhoefer, and K. Schmidt-Hoberg, (2014), arXiv:1412.5174 [hep-ph].
 - [41] P. Ball and R. Zwicky, Phys. Rev. **D71**, 014015 (2005), arXiv:hep-ph/0406232 [hep-ph].
 - [42] K. A. Olive *et al.* (Particle Data Group), Chin. Phys. **C38**, 090001 (2014).
 - [43] J. P. Lees *et al.* (BaBar), Phys. Rev. **D87**, 112005 (2013), arXiv:1303.7465 [hep-ex].
 - [44] W. Marciano and Z. Parsa, Phys.Rev. **D53**, 1 (1996).
 - [45] A. V. Artamonov *et al.* (E949), Phys. Rev. Lett. **101**, 191802

- (2008), arXiv:0808.2459 [hep-ex].
- [46] G. Ruggiero (NA62), *Proceedings, Kaon Physics International Conference (KAON13)*, PoS **KAON13**, 032 (2013).
- [47] R. Essig, A. Manalaysay, J. Mardon, P. Sorensen, and T. Volansky, *Phys.Rev.Lett.* **109**, 021301 (2012), arXiv:1206.2644 [astro-ph.CO].
- [48] R. Essig, J. Mardon, and T. Volansky, *Phys.Rev.* **D85**, 076007 (2012), arXiv:1108.5383 [hep-ph].
- [49] M. A. Shifman, A. I. Vainshtein, and V. I. Zakharov, *Phys. Lett.* **B78**, 443 (1978).
- [50] M. Cirelli, E. Del Nobile, and P. Panci, *JCAP* **1310**, 019 (2013), arXiv:1307.5955 [hep-ph].
- [51] D. S. Akerib *et al.* (LUX), *Phys. Rev. Lett.* **112**, 091303 (2014), arXiv:1310.8214 [astro-ph.CO].
- [52] R. Agnese *et al.* (SuperCDMS), *Phys. Rev. Lett.* **112**, 241302 (2014), arXiv:1402.7137 [hep-ex].
- [53] G. Angloher *et al.* (CRESTT), (2015), arXiv:1509.01515 [astro-ph.CO].
- [54] G. Gerbier, I. Giomataris, P. Magnier, A. Dastgheibi, M. Gros, *et al.*, (2014), arXiv:1401.7902 [astro-ph.IM].
- [55] P. Cushman, C. Galbiati, D. McKinsey, H. Robertson, T. Tait, *et al.*, (2013), arXiv:1310.8327 [hep-ex].
- [56] F. Bergsma *et al.* (CHARM), *Phys. Lett.* **B157**, 458 (1985).
- [57] S. Alekhin *et al.*, (2015), arXiv:1504.04855 [hep-ph].
- [58] R. Aaij *et al.* (LHCb), *JHEP* **02**, 105 (2013), arXiv:1209.4284 [hep-ex].
- [59] J. T. Wei *et al.* (Belle), *Phys. Rev. Lett.* **103**, 171801 (2009), arXiv:0904.0770 [hep-ex].
- [60] A. Alavi-Harati *et al.* (KTEV), *Phys. Rev. Lett.* **84**, 5279 (2000), arXiv:hep-ex/0001006 [hep-ex].
- [61] A. Alavi-Harati *et al.* (KTeV), *Phys. Rev. Lett.* **93**, 021805 (2004), arXiv:hep-ex/0309072 [hep-ex].
- [62] A. Djouadi, *Phys. Rept.* **457**, 1 (2008), arXiv:hep-ph/0503172 [hep-ph].
- [63] M. S. Turner, *Phys. Rev. Lett.* **60**, 1797 (1988).
- [64] J. A. Frieman, S. Dimopoulos, and M. S. Turner, *Phys. Rev.* **D36**, 2201 (1987).
- [65] A. Burrows, M. S. Turner, and R. P. Brinkmann, *Phys. Rev.* **D39**, 1020 (1989).
- [66] R. Essig, R. Harnik, J. Kaplan, and N. Toro, *Phys. Rev.* **D82**, 113008 (2010), arXiv:1008.0636 [hep-ph].
- [67] N. Ishizuka and M. Yoshimura, *Prog. Theor. Phys.* **84**, 233 (1990).
- [68] D. B. Kaplan, *Phys. Rev. Lett.* **68**, 741 (1992).
- [69] S. Nussinov, *Phys. Lett.* **B165**, 55 (1985).
- [70] S. M. Barr, *Phys. Rev.* **D44**, 3062 (1991).
- [71] S. M. Barr, R. S. Chivukula, and E. Farhi, *Phys. Lett.* **B241**, 387 (1990).
- [72] D. E. Kaplan, M. A. Luty, and K. M. Zurek, *Phys. Rev.* **D79**, 115016 (2009), arXiv:0901.4117 [hep-ph].
- [73] M. L. Graesser, I. M. Shoemaker, and L. Vecchi, *JHEP* **10**, 110 (2011), arXiv:1103.2771 [hep-ph].
- [74] T. Lin, H.-B. Yu, and K. M. Zurek, *Phys. Rev.* **D85**, 063503 (2012), arXiv:1111.0293 [hep-ph].
- [75] D. Tucker-Smith and N. Weiner, *Phys. Rev.* **D64**, 043502 (2001), arXiv:hep-ph/0101138 [hep-ph].
- [76] Y. Bai and T. M. P. Tait, *Phys. Lett.* **B710**, 335 (2012), arXiv:1109.4144 [hep-ph].
- [77] E. Izaguirre, G. Krnjaic, and B. Shuve, (2015), arXiv:1508.03050 [hep-ph].
- [78] B. Batell, D. McKeen, and M. Pospelov, *JHEP* **10**, 104 (2012), arXiv:1207.6252 [hep-ph].
- [79] P. Gondolo and G. Gelmini, *Nucl. Phys.* **B360**, 145 (1991).
- [80] E. W. Kolb and M. S. Turner, *Front. Phys.* **69**, 1 (1990).

APPENDIX A: HIGGS-MEDIATOR MIXING

In this appendix, we review the mixing ansatz chosen in the body of the paper. Following the notation in [78], above the scale of electroweak symmetry breaking, the most general renormalizable scalar potential for a SM Higgs doublet and scalar singlet is

$$V = V_H + V_\Phi + V_{\Phi H}, \quad (39)$$

where the contributions are

$$V_H = \mu_H^2 H^\dagger H + \lambda_H (H^\dagger H)^2 \quad (40)$$

$$V_\Phi = B_\Phi \Phi + \frac{\mu_\Phi^2}{2} \Phi^2 + \frac{A_\Phi}{3} \Phi^3 + \frac{\lambda_\Phi}{4} \Phi^4 \quad (41)$$

$$V_{\Phi H} = (A_{\Phi H} \Phi + \lambda_{\Phi H} \Phi^2) H^\dagger H. \quad (42)$$

For simplicity and without loss of essential generality, we choose $B_\Phi = A_{\Phi H} v^2 / 2$ to ensure that Φ does not receive a VEV. After electroweak symmetry breaking, Φ mixes with the scalar component of H and the mass matrix is

$$\mathbf{M}^2 = \begin{pmatrix} 2\lambda_H v^2 & A_{\Phi H} v \\ A_{\Phi H} v & \mu_\Phi^2 \end{pmatrix}, \quad (43)$$

which is diagonalized by the rotation

$$\begin{pmatrix} H \\ \Phi \end{pmatrix} = \begin{pmatrix} \cos \theta & \sin \theta \\ -\sin \theta & \cos \theta \end{pmatrix} \begin{pmatrix} h \\ \phi \end{pmatrix}, \quad (44)$$

where h is the physical Higgs boson, ϕ is the dark sector mediator, and

$$\tan 2\theta = \frac{2A_{\Phi H} v}{\mu_\Phi^2 - 2\lambda_H v^2}. \quad (45)$$

The mass eigenvalues in this setup are given by

$$m_{h,\phi}^2 = \frac{1}{2} \left(\mu_\Phi^2 + 2\lambda_H v^2 \pm \sqrt{F} \right), \quad (46)$$

where we have defined

$$F \equiv \mu_\Phi^4 + 4A_{\Phi H}^2 v^2 + 4v^4 \lambda_H^2 - 4\lambda_H \mu_\Phi^2 v^2. \quad (47)$$

Note that for appropriate choices of potential couplings in Eq. (40) it is always possible to engineer a sufficiently light scalar ϕ in the mass eigenbasis, though fine tuning may be required.

APPENDIX B: RELIC DENSITY COMPUTATION

To compute the relic density curve for the direct annihilation scenario, we begin by evaluating the total cross section $\sigma(s)$ for $\chi\bar{\chi} \rightarrow f\bar{f}$ annihilation which recovers Eq. (5) in the nonrelativistic limit. Performing the thermal average [79]

$$\langle \sigma |v| \rangle_{\chi\bar{\chi} \rightarrow f\bar{f}} = \frac{1}{N_\chi} \int_{4m_\chi^2}^{\infty} ds \sigma(s) (s - 4m_\chi^2) \sqrt{s} K_1 \left(\frac{\sqrt{s}}{T} \right), \quad (48)$$

where $N_\chi = 8m_\chi^4 T K_2^2(m_\chi/T)$ and K_n is a Bessel function of the n^{th} kind. The annihilation cross section is

$$\sigma(s)_{\chi\chi \rightarrow f\bar{f}} = \frac{g_\chi^2 g_f^2 s}{16\pi(s - m_\phi^2)^2} \sqrt{1 - \frac{4m_f^2}{s}} \left(1 - \frac{4m_\chi^2}{s}\right)^{3/2}, \quad (49)$$

where the mediator-SM coupling depends on the available hadronic thresholds accessible for a given value of s . Near Λ_{QCD} , we model this coupling as [29]

$$g_f(s) \simeq \sin\theta \sqrt{\frac{8\pi}{m_h} \Gamma(h \rightarrow \text{SM})} \Big|_{m_h=\sqrt{s}}, \quad (50)$$

and have checked that for \sqrt{s} away from Λ_{QCD} , where the final states consist only of elementary particles, this procedure matches onto the analytical result computed using only SM yukawa couplings.

Following the procedure in [80], the relic abundance of χ is

$$\Omega_\chi h^2 = 1.07 \times 10^9 \frac{\sqrt{g_*} (n+1) x_f \text{GeV}^{-1}}{g_{*,s} m_{Pl} \langle \sigma|v| \rangle_f}, \quad (51)$$

where $n = 0, 1$ for s and p wave annihilation, g_* and $g_{*,s}$ are respectively the relativistic and entropic degrees of freedom, $x \equiv m_\chi/T$, and an f subscript denotes a freeze out value.

APPENDIX C: THERMALIZATION CRITERIA

To produce DM thermally in equilibrium, at minimum we require the production rate to exceed the expansion rate at some point in the early universe, $n_f(T) \langle \sigma|v| \rangle_{f\bar{f} \rightarrow \chi\bar{\chi}} \gtrsim H(T)$, where n_f is the fermion number density and $H(T) \simeq 1.66 \sqrt{g_*} T^2 / m_{Pl}$. Per SM fermion species f , the cross section for annihilation is

$$\sigma(s)_{f\bar{f} \rightarrow \chi\bar{\chi}} = \frac{g_\chi^2 g_f^2 s}{16\pi(s - m_\phi^2)^2} \sqrt{1 - \frac{4m_\chi^2}{s}} \left(1 - \frac{4m_f^2}{s}\right)^{3/2}, \quad (52)$$

The thermal average is

$$\langle \sigma|v| \rangle_{f\bar{f} \rightarrow \chi\bar{\chi}} = \frac{1}{N_f} \int_{4m_\chi^2}^{\infty} ds \sigma(s) (s - 4m_f^2) \sqrt{s} K_1\left(\frac{\sqrt{s}}{T}\right), \quad (53)$$

where $N_f = 8m_f^4 T K_2^2(m_f/T)$. At very high temperatures, the number densities scale as $n_f(T) \langle \sigma|v| \rangle \propto T$, whereas $H(T) \propto T^2$ so as the universe cools, the thermal production rate increases relative to Hubble. In the opposite, non relativistic regime, the number density falls exponentially $n_f(T) \propto \exp(-m_f/T)$ so the rate decreases sharply relative to Hubble, which still scales as T^2 during radiation domination. The total rate for comparison with Hubble is

$$\Gamma_{\text{SM} \rightarrow \chi\bar{\chi}} = \sum_f n_f(T) \langle \sigma|v| \rangle_{f\bar{f} \rightarrow \chi\bar{\chi}}, \quad (54)$$

which we compare with the Hubble rate $\Gamma_{\text{SM} \rightarrow \chi\bar{\chi}}$ near $T \sim m_t$ because this is the temperature at which the leading production cross section ($t\bar{t} \rightarrow \chi\bar{\chi}$) no longer scales as T^{-2} but acquires m_t dependence from the propagator as $s \approx 4m_t^2$.

APPENDIX D: THREE BODY MESON DECAYS

For $m_\phi > m_{B^+} - m_{K^+}$, it is still possible for DM to contribute to rare B decays through $B \rightarrow K\bar{\chi}\chi$ via virtual ϕ exchange. The width for this process can be computed as a convolution of 2 body processes, treating the intermediate ϕ propagator as a Breit-Wigner function

$$\Gamma_{B^+ \rightarrow K^+ \chi\bar{\chi}} = \int_{4m_\chi^2}^{0.3 m_B^2} dq^2 \Gamma_{B^+ \rightarrow K^+ \phi}(q^2) F(q^2), \quad (55)$$

where we define

$$F(q^2) = \frac{m_\phi \Gamma_\phi / \pi}{(q^2 - m_\phi^2)^2 + m_\phi^2 \Gamma_\phi^2}, \quad (56)$$

$$\Gamma_\phi \equiv \Gamma(\phi \rightarrow \chi\bar{\chi}) = \frac{g_\chi^2 m_\phi}{8\pi} \left(1 - \frac{4m_\chi^2}{m_\phi^2}\right)^{3/2}, \quad (57)$$

such that F is normalized to recover a delta function in the vicinity of m_ϕ as $\Gamma_\phi \rightarrow 0$ limit. The upper integration limit in Eq. (55), $q^2 = 0.3 m_B^2$, is chosen in accordance with the cut imposed in [43]. An analogous expression is used to compute the width for $K^+ \rightarrow \pi^+ \chi\bar{\chi}$ using the cuts in [45], which constitutes the right most region of the orange shaded contour in Fig. 2.